

# A Side-Effect-Free Interventional Therapy for Precisely Eliminating Unresectable Cancer Pain

Pengfei Zhang,\* Sheng Yao, Yu Tang, Shanhe Wan, Xiaoyuan Chen,\* and Li Ma\*



Cite This: *ACS Nano* 2023, 17, 23535–23544



Read Online

ACCESS |

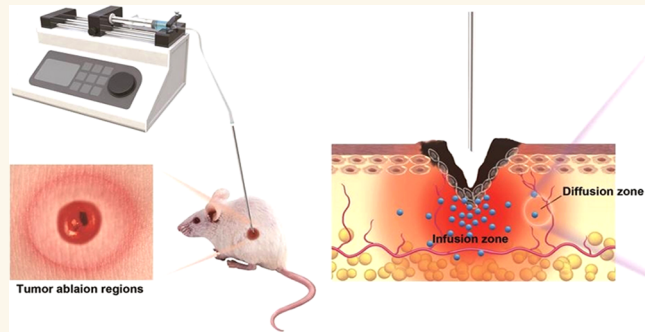
Metrics & More

Article Recommendations

Supporting Information

**ABSTRACT:** Of patients bearing unresectable tumors at advanced stages, most undergo serious pain. For unresectable tumors adjacent to vital organs or nerves, eliminating local cancer pain without adverse effects remains a formidable challenge. Interventional ablative therapies (IATs), such as radio frequency ablation (RFA), microwave ablation, and irreversible electroporation, have been clinically adopted to treat various carcinomas. In this study, we established another palliative interventional therapy to eliminate local cancer pain, instead of relieving nociception temporarily. Here, we developed another interventional ablative therapy (termed nanoparticle-mediated microknife ablation) to locoregionally eliminate cancer pain and tumors. The IAT system was composed of self-assembled nanodrugs, infusion catheters, puncture needles, injection pump, and an empirical tumor ablation formula. Notably, the ablation formula established in the IAT system enables us to predict the essential nanoparticle (NP) numbers used for completely destroying tumors. In a mouse model of cancer pain, tumor-targeted nanodrugs made of Paclitaxel and Hematoporphyrin, which have an extremely high drug-loading efficiency (more than 60%), were infused into tumors through injection pumps under imaging guidance. In conclusion, when compared to classic chemotherapeutic agents, IAT showed significantly higher effectiveness in cancer pain removal. It also presented no damage to the nervous, sensory, and motor capabilities of the treated mice. All of these merits resulted from NPs' long-lasting retention, targeted ablation, and confined diffusion in tumor stroma. Therefore, this safe treatment modality has great potential to eradicate local cancer pain in the clinic.

**KEYWORDS:** *cancer pain, pain treatment, interventional nanomedicine, precision nanomedicine, carrier-free nanoparticles, drug coassembly*



Despite improvement in pain management, 70% of patients bearing advanced malignancies suffer from cancer-related pain.<sup>1–3</sup> Clinical outcomes of cancer pain control tend to be poor in many patients.<sup>4</sup> This places unendurable physiological and psychological burdens on those sufferers, even accelerating disease progression.<sup>4</sup> These sufferings apparently weaken patients' willingness to survive, but attention toward the issue seems inadequate.<sup>4,5</sup>

One of the major types of cancer pain is deemed to be neuropathic pain,<sup>5,6</sup> which can be attributed to peripheral nerve compression by neoplasms. When possible, the pain sources were removed by surgical resection. Unfortunately, for a large proportion of patients in the terminal stage of cancer, lesions are frequently unresectable because of tumor invasion into vital organs or nervous systems.<sup>7,8</sup> Although opioid drugs act as cornerstones of pain control in advanced cancer cases,<sup>1</sup> cancerous neuropathic pain is often intractable.<sup>9</sup> On the other

hand, the negative effects of opioid analgesics involve nausea, apnea, addiction, sedation, and drug tolerance risk.<sup>10,11</sup> These drawbacks further impede their practical application. Moreover, palliative treatments using analgesic drugs merely give rise to short-term action and frequently fail to produce sufficient analgesia efficacy.<sup>11,12</sup>

Nanotechnology-based strategies have been utilized to tackle various pain diseases; the studies about cancer pain relief using nanocarriers are still rare.<sup>13–18</sup> Overall, previous studies

**Received:** July 15, 2023

**Revised:** November 9, 2023

**Accepted:** November 13, 2023

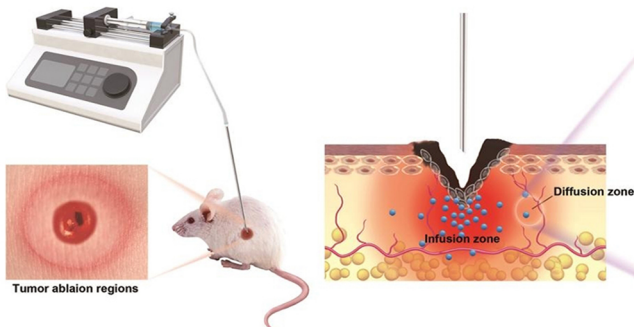
**Published:** November 21, 2023



regarding cancer pain management always focused on transitory ache relief but not pain eradication.<sup>19–24</sup> In addition, interventional ablative therapies (IATs), including microwave ablation, radiofrequency ablation (RFA), and irreversible electroporation, have been clinically applied in treating a wide range of carcinomas. However, insufficient ablation produced by conventional IAT may cause tumor recurrence. Besides, during thermal ablative therapies, tumor locations close to vital organs likely bring about severe injuries to surrounding healthy tissues. Hence, the application field of IAT is indeed limited, and only a fraction of patients can benefit from this technique. More powerful and safe IAT must be exploited urgently.

Taken together, a nonaddictive, long-lasting, safe, and efficient approach to removing advanced cancer pain is elusive currently.<sup>3,11,21,23,25,26</sup> Eradicating locoregional tumors and cancer pain safely remains a significant challenge.<sup>27–29</sup> Therefore, to surmount the above-mentioned challenges, we developed another IAT termed nanoparticle-mediated microknife (NP-MK) ablation to locoregionally eliminate cancer pain as well as tumors. This IAT system was composed of self-assembled nanoparticles (NPs), infusion catheters, puncture needles, injection pump, and an empirical tumor ablation formula. In a cancer pain model,<sup>30</sup> high drug-loading efficiency (DLE) of nanodrugs composed of Paclitaxel (PTX) and Hematoporphyrin (HP) were directly infused into tumors *via* puncture needles and injection pumps under imaging guidance, which thus made intratumoral (*i.t.*) administration more accurate. With the aid of targeted ligand HP, the self-assembled nanodrugs can discriminate between cancerous and normal cells around injection sites, safely achieving tumor-specific ablation (Scheme 1).

**Scheme 1. An Interventional Ablative Therapy (IAT) Termed Nanoparticle-Mediated Microknife Ablation Is Successfully Set up to Eliminate Cancer Pain and Tumors Locoregionally under Imaging Guidance<sup>a</sup>**



<sup>a</sup>The IAT approach presents favorable therapeutic efficacy and shows no damage to nervous, sensory, and motor functions of treated mice, largely owing to long-term retention, targeted ablation, and confined diffusion of nanoparticles in tumor regions.

Notably, it was found that absolute NP numbers ( $N_{NPs}$ ) have an approximately linear correlation with the tumor volume reduction ( $V_{reduction}$ ). In virtue of the acquired function correlation, we could predict essential NP amounts to precisely destroy lesions. In this way, the NP-MK system was used to eradicate local cancer pain, and it showed no detectable toxicity to neighboring healthy tissues. This technique also presents no obvious damage to nervous, sensory, and motor

functions of treated mice. In addition, pain-relevant symptoms fully disappeared in mice after IAT treatments. Thus, we successfully set up an interventional ablative therapy (IAT) to eradicate local cancer pain at an advanced stage. This NP-MK technique may provide an alternative avenue for expanding application fields of nanomedicine. It can be expected that all kinds of nanocarriers will be developed prosperously for precise IAT by utilizing analogous patterns to NP-MK systems.

## RESULTS

**Synthesis and Characterization of Carrier-Free Nanodrugs.** The carrier-free nanodrugs having a high drug loading efficiency (DLE) were prepared using a nanoprecipitation method. Briefly, paclitaxel (PTX) and hematoporphyrin (HP) were dissolved together in dimethyl sulfoxide (DMSO), followed by addition of the mixture to physiological saline containing polyvinylpyrrolidone (PVP) under the condition of stirring vigorously. Because of the solvent variation, PTX and HP molecules coassembled quickly to form PTX nanoparticles (termed PTX-HP nanodrugs). Then, after dialysis and centrifugation separation, the resulting nanoparticles (NPs) were acquired facilely. The integration of HP into the nanoformulation guarantees the NPs' good dispersity.

Through attempting various ratios of formulations, we obtained optimal PTX-HP nanodrugs after coassembly of PTX and HP molecules at a mass ratio of 4:1, which thus possessed a very high DLE (~63%), favorable polydispersity (0.11 to 0.15), and uniform morphologies of nanospheres (Figure S1A). As monitored by dynamic light scattering (DLS) (Figure S1B,C), PTX-HP nanodrugs also exhibited excellent stabilities (in a salt solution, 0.1% NaCl) as well as a hydrodynamic diameter of about 95 nm. By utilizing phosphate-buffered saline (PBS) plus 10% fetal bovine serum (FBS) to imitate physiological environments, we observed a long-lasting PTX release from NPs *in vitro* over a period of three weeks. Furthermore, the NPs could be efficiently internalized in tumor cells, thereby eliciting strong cellular toxicities similar to equivalent doses of PTX agents (Figure S1D,E). According to high-sensitive Flow NanoAnalyzer measurements, the purified PTX-HP nanoformulation (made of 1.89 mg mL<sup>-1</sup> PTX) contained  $1.61 \times 10^{12}$  NPs in 1 mL of solution. Unless otherwise specified, this nanodrug concentration was used in subsequent experiments. A mass ratio of four (PTX/HP) would be adopted in nanodrug fabrication in order to obtain ideal nanoparticles (about 100 nm in diameter). Amphiphilic HP is a negatively charged dispersing agent that facilitates hydrophobic PTX as a core to form stable nanodrugs. HP is also considered to be located on the NPs' outside surfaces when it is used in nanodrug fabrication, largely resulting in its high stabilities.

**Orthotopic Tumors Are Eliminated Precisely in Cancer Pain Models by Employing the Established NP-MK System.** Next, to ensure the accuracy and reproducibility of intratumoral (*i.t.*) administration, we adopted an injection pump device equipped with puncture needles to conduct all drug infusions. By employing a hyaluronate acid (HA) hydrogel to simulate tumor stroma tissues, we found that a low injection rate (less than 10  $\mu\text{L s}^{-1}$ ) contributed to the production of more regular infusion shapes when compared to fast liquid afflux (Figure 1A). Drug extravasation from HA hydrogel likely occurred at a high infusion rate. Therefore, the subsequent interventional administration would be performed through injection pumps

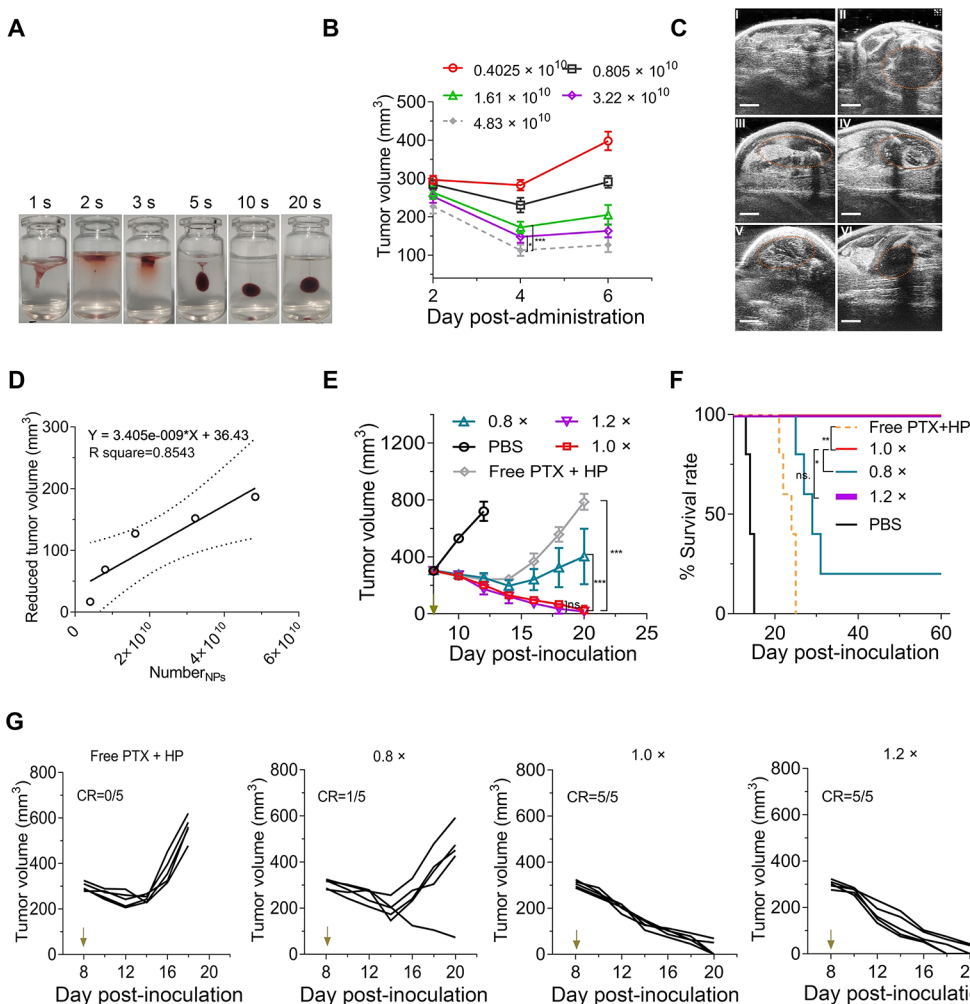


**Figure 1.** Orthotopic tumors are cleared up precisely in cancer pain models by the use of NP-MK system under US imaging guidance. (A) Representative images show that infusion of nanoparticles using the NP-MK system at different rates (a  $100 \mu\text{L}$  dose for 1, 2, 3, 5, 10, or 20 s) yields various infusion shapes in HA hydrogels. (B) Tumor volume changes in mouse models of cancer pain after intratumoral (i.t.) infusions of different doses (i.e.,  $0.4025 \times 10^{10}$ ,  $0.805 \times 10^{10}$ ,  $1.61 \times 10^{10}$ ,  $3.22 \times 10^{10}$ , or  $4.83 \times 10^{10}$  NPs) of nanodrugs by the NP-MK system. (C) On Day 4 after interventional administration of  $0.4025 \times 10^{10}$  (II),  $0.805 \times 10^{10}$  (III),  $1.61 \times 10^{10}$  (IV),  $3.22 \times 10^{10}$  (V), or  $4.83 \times 10^{10}$  (VI) NPs, representative US images show sham normal groups (I) and sarcoma (II to VI); yellow circles denote tumor regions measured by ultrasonography. Scale bars, 4 mm. (D) Linear regression analysis between NPs' numbers ( $N_{NP}$ ) and tumor volume reduction ( $V_{reduction}$ ) on the fourth day after treatments ( $R^2 = 0.8345$ ). (E) Tumor growth profiles of cancer pain models receiving a single administration of PBS, free PTX + HP, or nanoparticles (0.8×, 1.0×, or 1.2× the benchmark dose of NPs). The linear regression equations are employed to calculate NP benchmark doses ( $Y = 3.405e-009X + 36.43$ ; If the  $Y$  value is 300, NP benchmark amounts served as  $X$  values can be obtained by using this function). (F) Mouse survival curves after various treatments. (G) Individual tumor growth graphs from E indicating complete tumor regression rates (CR). Brown arrows represent a single interventional administration *via* injection pumps on the eighth day after inoculation. \* $P < 0.05$ , \*\* $P < 0.01$ , and \*\*\* $P < 0.001$ . Statistical differences were compared with a two-way analysis of variance (ANOVA) for (B) and (E). Mantel-Cox test was conducted for survival analysis (F). All data were exhibited as means  $\pm$  SD ( $n = 5$ ). ns means not significant.

at a flow rate of  $5 \mu\text{L s}^{-1}$  under imaging guidance. After that, by inoculation of S180 sarcoma cells to the immediate vicinity of the sciatic nerve, we established a mouse model of cancer pain following ultrasound (US) examination. As previously reported, this animal model presented classic symptoms of spontaneous cancer pain (hind paw-lifting actions) and stimulus-elicited hyperalgesia as a result of nerve compression by orthotopic tumors.

When the sarcoma volume approximated to  $280 \text{ mm}^3$ , a puncture needle was inserted into central regions of tumors under the direction of US imaging, followed by i.t. infusion of nanodrugs (i.e.,  $0.4025 \times 10^{10}$ ,  $0.805 \times 10^{10}$ ,  $1.61 \times 10^{10}$ ,  $3.22 \times 10^{10}$ , and  $4.83 \times 10^{10}$  NPs) *via* injection pumps (Figure 1B).

As shown in Figure 1B, tumor sizes gradually decreased after interventional therapies. US images revealed that the reduction in tumor volume reached a maximum in all treated groups on the fourth day after treatments (Figure 1C), but tumors began to regrow following initial regression (Figure 1B). Considering that a lack of administration doses might lead to tumor residues, we further analyzed the correlation between NPs' absolute numbers ( $N_{NP}$ ) and tumor volume reduction ( $V_{reduction}$ , on the fourth day after treatments) to predict essential doses used for eradicating local neoplasms. US imaging was also employed to detect neoplasm size changes. Ultimately, a linear regression analysis was carried out between  $N_{NP}$  and  $V_{reduction}$  (Figure 1D). The relation coefficient ( $R$ ) and

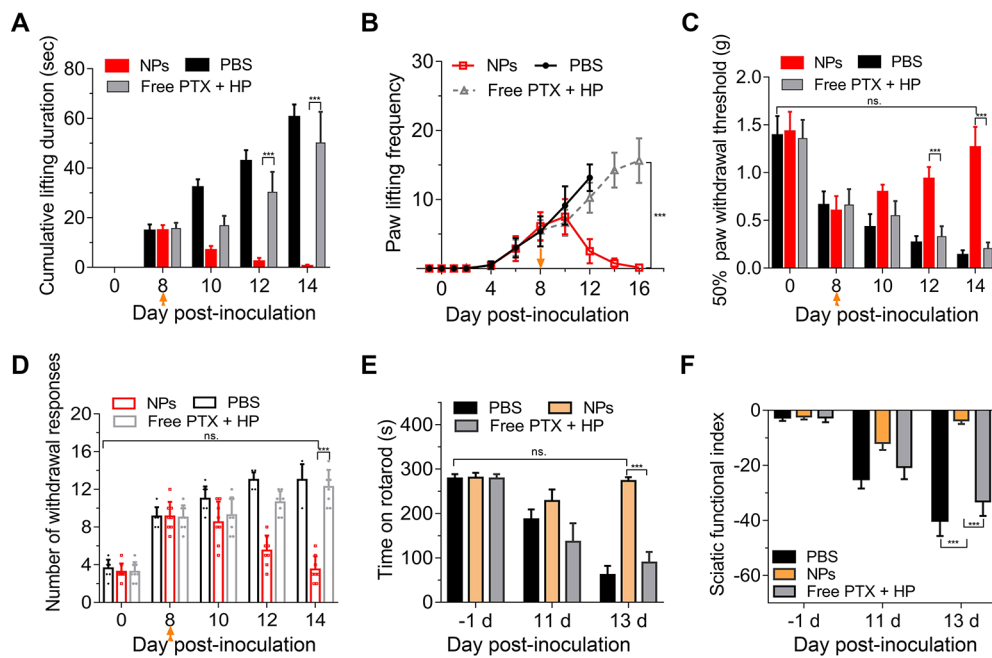


**Figure 2.** NP-MK system using targeted nanodrugs further eliminates cancer pain without detectable side effect. After interventional treatments, cancer pain symptoms, such as (A) cumulative paw-lifting time, (B) mouse paw-lifting frequency, (C) hyperalgesia against mechanical stimuli, and (D) cold hypersensitivity, are inspected, respectively. (E) Motor abilities of mice receiving interventional administration of PBS, NPs, or free PTX plus HP are assessed in rotarod assays. (F) After interventional treatments with different formulations, the nervous functions were further revealed by measuring sciatic function indexes in cancer pain models. Yellow arrows suggest a single interventional administration under US imaging guidance on Day 8 after inoculation. \* $P < 0.05$ , \*\* $P < 0.01$ , and \*\*\* $P < 0.001$ .  $P$  values were calculated by an unpaired two-tailed  $t$  test in (A–F) (means  $\pm$  SD;  $n = 6$  to 8). ns means not significant.

linear regression equations were acquired from Figure 1D. Comfortably, the relatively high  $R^2$  values ( $R^2 = 0.8534$ ) suggested a good linear correlation between  $N_{NP}$  and  $V_{reduction}$ .

Thereafter, in order to further investigate the applicability of this linear regression equation, tumors (around  $300 \text{ mm}^3$ ) in cancer pain models were infused with a single dose of PBS, free PTX + HP, or nanodrugs under US imaging guidance. The administration doses were, respectively, 0.8, 1.0, and  $1.2 \times$  the NP benchmark numbers ( $N_{NP}$ ) calculated from the linear regression equation. [i.e.,  $Y = 3.405e-009*X + 36.43$ ; if tumor volume reduction ( $Y$  value) is 300, benchmark NP numbers ( $N_{NP}$ ,  $X$  value) can be obtained from the equation. Finally,  $N_{NP}$  is determined to be  $7.741 \times 10^{10}$ .] Tumor progression after percutaneous injection was also assessed by applying US imaging. At Day 20 after tumor inoculation, US measurements proved evident tumor growth in mice treated with free PTX + HP, or low doses ( $0.8 \times N_{NP} = 6.193 \times 10^{10}$  NPs) of nanoformulation (Figure 1E). In contrast, the mice receiving 1.0 or  $1.2 \times$  the basic doses of nanoparticles ultimately showed no detectable tumor (Figure 1E). As documented in Figure 1F, the mice treated with a benchmark dose ( $1.0 \times N_{NP} = 7.741 \times 10^{10}$  NPs) of nanodrugs exhibited a long survival time (over 54 days) similar to ones receiving  $1.2 \times$  the basic dose of NPs ( $1.2 \times N_{NP} = 9.289 \times 10^{10}$  NPs), and no tumor relapse was observed in the two groups. On the contrary, malignancy relapse occurred frequently in groups receiving  $0.8 \times$  the benchmark dose of NPs (4/5) or PTX plus HP agents (5/5), which ultimately led to significantly short survival time (Figure 1F,G). Furthermore, Figure 1G established that sufficient administration doses, including 1.0 and  $1.2 \times$  the basic doses of NPs, enabled lesions to be fully cleared (100% tumor regression rate,  $n = 5$  per group). Taken together, all results substantially verified that the established IAT system was

available in animal models of orthotropic sarcomas. Depending on the linear regression equation ( $Y = 3.405e-009*X + 36.43$ ) from Figure 1D, we could calculate basic NPs' numbers/doses ( $N_{NP}$ , defined as  $X$  values) to precisely eliminate tumors. The slope of the linear regression equation was defined as tumor-killing coefficients (namely,  $\kappa$  values) to reflect NPs' antitumor capacities.

**The NP-MK System Using Targeted Nanodrugs Eradicates Local Cancer Pain as well as Sarcoma In Situ.** To estimate the potency of the NP-MK system in cancer pain removal, we employed another batch of mouse models bearing cancer pain in subsequent behavioral assays ( $n = 6$  to 8 for each group). On the eighth day after tumor inoculation, the mice developed signs of lifting their hind paw, which was associated with spontaneous pain. Then, the tumors (around  $300 \text{ mm}^3$ ) were percutaneously infused with PBS, free PTX + HP, or a basic dose ( $1.0 \times N_{NP} = 7.741 \times 10^{10}$  NPs) of nanodrugs under ultrasonography piloting. At predesigned time points, researchers recorded the cumulative duration and paw-lifting frequency in each mouse during a 10 min observation period (Figure 2A,B). Figure 2A showed that paw-lifting actions gradually disappeared in nanodrug-treated groups, whereas the symptom of spontaneous cancer pain became more and more obvious (up to around 47 s on Day 14) in PTX-treated mice. No paw-lifting behavior was found in the contralateral hind limbs.

These data documented that the NP-MK ablation can be used for eradicating spontaneous cancer pain (Figure 2A,B). Also, we probed the ability of the NP-MK system to alleviate mechanical allodynia as well as hyperalgesia. Following various treatments, mechanical hypersensitivity was assessed in von Frey tests where hind paws were irritated with von Frey filaments, generating a series of forces (0.04–2.00 g) so as to

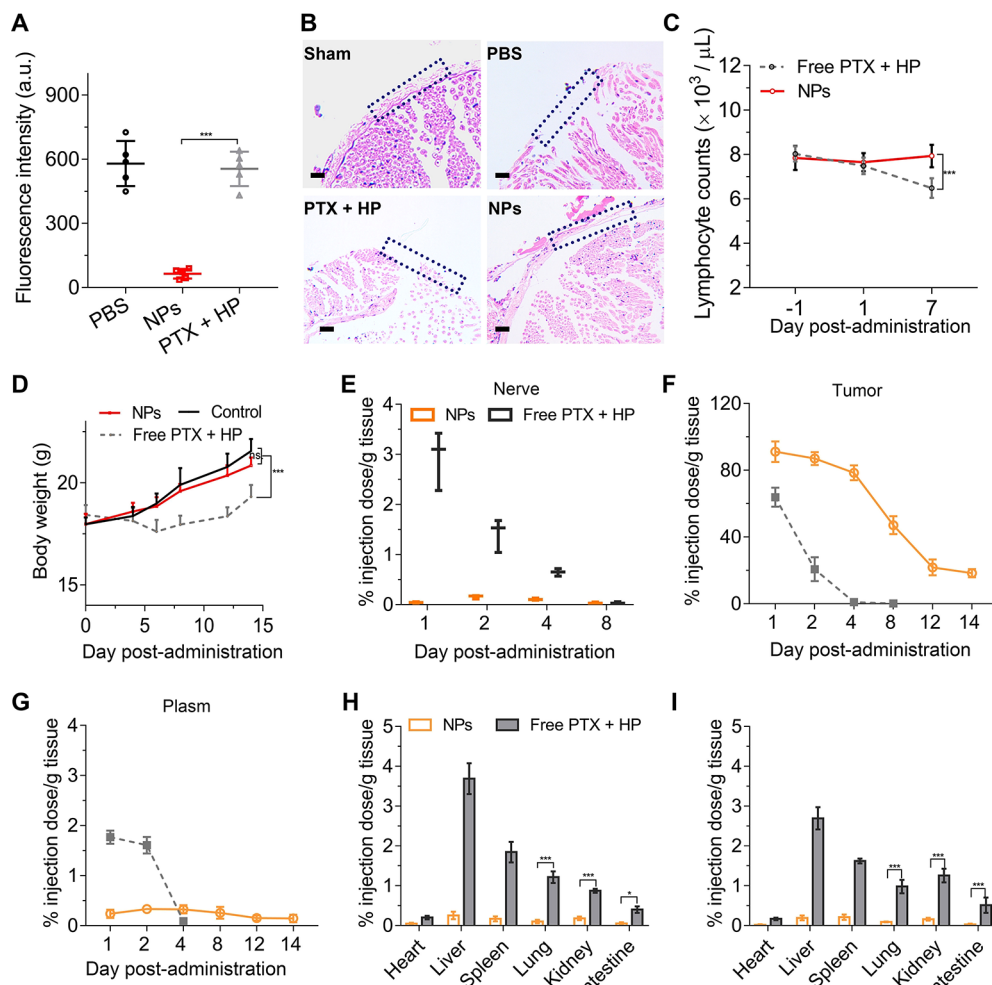


**Figure 3.** NP-MK system does not elicit severe side effects (nerve injuries) in cancer pain treatments, largely attributed to long-term retention and confined diffusion of nanodrugs within tumors. (A) The penetration of ICG dyes into sciatic nerves indicates structural integrity of epineurium in cancer pain models after interventional treatments with PBS, NPs, or free PTX + HP. (B) Representative H&E-stained sections of sciatic nerves in mice bearing cancer pain. Blue boxes also unveil peripheral structures of sciatic nerves on Day 16 after tumor inoculation ( $n = 5$ ). The scale bar indicates  $50 \mu\text{m}$ . (C, D) Detection of (C) lymphocyte counts and (D) body weights in normal mice treated with nanodrugs or an equivalent dose of PTX plus HP. (E–G) Quantitative measurements of PTX contents in (E) sciatic nerves, (F) orthotopic tumors, or (G) plasma using LC-MS/MS analysis after different interventional treatments ( $n = 3$ ). (H, I) Quantitation of PTX distribution in vital organs by LC-MS/MS at (H) 24 h or (I) 48 h following interventional administration,  $n = 3$ . \* $P < 0.05$ , \*\* $P < 0.01$ , and \*\*\* $P < 0.001$ . Statistical difference was checked using a two-tailed unpaired  $t$  test for (A) or with a two-way analysis of variance (ANOVA) for (C–I). All data represent the means  $\pm$  SD. ns means not significant.

calculate 50% withdrawal thresholds (Figure 2C). For the PBS group bearing cancer pain, paw withdrawal thresholds exhibited a trend to gradually diminish, indicating the augmented sensitivity to mechanical irritations. On Day 14 after inoculation, withdrawal thresholds of ipsilateral paws in NP-treated mice and in PTX-treated groups were  $1.26 \pm 0.22$  and  $0.20 \pm 0.07$  g, respectively (Figure 2C). Notably, no significant difference was found between the NP group and the tumor-free control group.

Next, by dropping acetone to the plantar surface of the hind paw, we further monitored the cold hypersensitivity in the cancer pain models. Paw withdrawal frequency was recorded following acetone stimulation (Figure 2D). For tumor groups, paw withdrawal responses gradually became frequent. On the contrary, the mice subjected to nanodrug treatments presented an apparent decrease in acetone-elicited hypersensitivity, as reflected in Figure 2D. At Day 14, paw-withdrawing responses in PTX plus HP-treated mice were 2.5-fold higher when

compared to ones receiving NP administration (Figure 2D), implying its hypersensitivity to cold stimulation. All data suggested that the IAT using NP-MK systems indeed had the capacity to eradicate local cancer pain.

**The Established IAT Shows a Negligible Injury to Nervous, Sensory, and Motor Functions of Treated Mice.** Given its powerful potency, we further examined the impact of the NP-MK system on nervous functions. We first conducted rotarod assays to determine mouse retention time on rotating rods, which denotes motor functions of the treated mice. On Day 13 after inoculation, Figure 2E (rotarod tests) demonstrated a full recovery of motor functions in the NP-treated group, whereas the mice in the presence or absence of PTX plus HP treatments obviously developed motor dysfunction on Day 11. In footprint assays (Figure 2F), the sciatic function index (SFI) was measured to evaluate basic functions of sciatic nerves. Consistent with the results of rotarod assays, PTX plus HP treatments gave rise to an evident

reduction in SFI, which thus revealed a severely impaired condition of sciatic nerves, while the mice receiving the benchmark dose ( $1.0 \times N_{NP} = 7.741 \times 10^{10}$  NPs) of nanodrugs presented a high score of SFI on Day 13 (Figure 2F).

Subsequently, the tumor residues were resected after various treatments and stained with hematoxylin and eosin (H&E). Representative histological pictures (Figure S2) confirmed that no classic cancer cell was seen in NP-treated groups, further proving the entire clearance of tumors by the NP-MK system.

**NP-MK System Presents a Good Biosafety, Inducing No Detectable Side Effect.** When all behavioral tests were accomplished on the 16th day after tumor inoculation, we assessed the side effects of the NP-MK system. Eight hours after i.t. injection of fluorescent dyes indocyanine green (ICG), the sciatic nerves close to neoplasms were harvested and subjected to quantitative detection of ICG fluorescence, followed by staining with hematoxylin and eosin (H&E). As illustrated in Figure 3A, the sciatic nerves in the PBS group (PBS treatment) had 8.95-fold higher fluorescence signals than that of NP-treated nerves. Figure 3B also documented that the penetration of ICG dye into sciatic nerves in the PTX plus HP group was likely due to epineurium structure impairments. Intratumoral infusion of NPs induced no notable damage to the treated sciatic nerves (Figure 3B). In addition, PTX plus HP treatments seemed to be insufficient to prevent epineuria from destruction by sarcoma cells. There were evident defects in nervous myelin sheaths of tumor-bearing mice (PBS group, Figure 3B) on Day 16 after tumor inoculation.

To inspect NPs' toxicities to healthy mice, we conducted a hematological analysis after a single intramuscular (i.m.) administration and then found no marked change in key health indicators (Figure S3A–D) such as aspartate aminotransferase (AST), alanine aminotransferase (ALT), urea nitrogen concentration, mean corpuscular hemoglobin concentration (MCHC), hemoglobin (HGB), and red blood cell levels (RBCs). Besides, PTX plus HP administration elicited a significant reduction in total lymphocytic numbers on the seventh day after treatments, while the mice receiving NP-MK therapies exhibited negligible changes in lymphocyte counts (Figure 3C). Body weights were increased in NP-treated mice, analogous to the control groups (Figure 3D). In summary, these results validated that NP-MK therapies had exciting superiorities over conventional chemotherapeutics due to its favorable efficacy in safely eradicating local malignancies and cancer pain.

**Size-Exclusion Effects of Nanodrugs in Tumor Stroma Play Critical Roles in NPs' Long-Lasting Retention and Confined Diffusion, Thus Yielding Satisfactory Therapeutic Efficacy.** To further explore the reasons for its favorable biosafety and therapeutic potency, we inspected the biodistribution of nanodrugs after NP-MK treatments. Briefly, another batch of mice bearing cancer pain was randomly separated into 2 groups and then received i.t. administration of nanodrugs ( $1.0 \times N_{NP}$ ) or free PTX plus HP. At predetermined time points, tumors and vital organs of these mice were resected to measure PTX contents by liquid chromatography with tandem mass spectrometry (LC-MS/MS) analysis.

In biodistribution experiments, PTX levels were dramatically lower in nerve tissues of NP-treated mice than in PTX plus HP groups (Figure 3E). Figure 3E showed that when compared to small-molecule drugs like PTX, it was more difficult for large-sized nanoparticles to infiltrate into nervous fibers, regardless

of nerve sheath barriers. Furthermore, PTX plus HP infusion only preserved about 23% of total PTX contents in tumors on Day 2, followed by complete clearance within 4 days. In contrast, NP deposits kept over 40% of payloads in neoplasms for 8 days (Figure 3F). More importantly, on the 14th day after nanodrug infusion ( $n = 3$  each time point), there was still 18% of initial injection doses in harvested tumors. Therefore, it can be concluded that NP-MK treatments gave rise to long-term NPs' retention in tumors over 14 days (Figure 3F), and a high nanodrug concentration in tumors contributed to the removal of cancer pain. Upon i.t. administration, the small-molecule drug PTX was prone to dissemination from orthotopic neoplasms, which largely triggered tumor recurrences. Besides, after locoregional treatments with free PTX plus HP agents, high levels of PTX accumulated in the mouse plasma (Figure 3G), liver, spleen, lung, and kidney (Figure 3H,I). The mice treated with free PTX + HP showed a similar drug level in plasma between Day 1 and Day 2 (Figure 3G), which can be attributed to intratumoral administration of free PTX in DMSO as well as a relatively slow release of hydrophobic PTX in tumor tissues.

Intriguingly, the injected nanodrugs tended to be retained in tumor tissues and exhibited low levels of PTX dissemination to mouse organs at 24 and 48 h after administration (Figure 3H,I). The NPs' diffusion seemed confined in tumor regions, thereby ensuring the safety of this IAT.

## CONCLUSION

As locoregional tumor masses were eliminated by the use of the NP-MK system, the signs of cancer pain had disappeared in treated mice, which suggested that the interventional precision treatments indeed eradicated local cancer pain at terminal stages. Notably, the NP-MK therapies were dramatically effective in cancer pain removal, whereas free PTX revealed a slight potency to attenuate sufferings. We found that manual injection manners very easily lead to drug extravasation from injection sites and that rapid intravenous (i.v.) injection often triggers the drug extravasation from tumors. Mechanical injection modes enable extremely slow i.t. infusion, which has better reproducibility and precision when compared to manual injection. As a result, the use of mechanical pump-injection is an important basis of improving administration precision as well as the tumor ablation formula.

The advantages of this IAT system over conventional chemotherapeutics (PTX) primarily arise from NPs' excellent features that enable PTX-HP nanoparticles to actualize long-term retention and locally confined diffusion in tumors, which are distinct from small-molecule drugs.<sup>26</sup> Besides, size-exclusion effects of nanoparticles in tumor stroma or around myelinated nerves prohibit their further dissemination from neoplasms to other important organs.<sup>27</sup> The long-term retention and confined diffusion of nanoparticles within tumor regions also play critical roles in clearing up cancer pain without a negative effect.<sup>30</sup> It has been demonstrated that hematoporphyrin derivative was tumor-selective and accumulated specifically in malignant tissues, which was utilized as a targeted ligand to distinguish neoplasms from healthy organs in the NP-MK system.<sup>31,32</sup> More importantly, we found that the absolute numbers ( $N_{NP}$ ) of NPs have an approximately linear relation with tumor ablation volume by use of the NP-MK system. The method we established was also proved to predict the necessary NP amounts that enable the complete elimination of local tumors and cancer pain. In conclusion,

another IAT method using the NP-MK system was clarified to realize precise local tumor eradication. Therefore, it can be expected that the therapeutic approach has excellent potential for conquering advanced cancer pain in the clinic and it will likely benefit more cancer patients in the future.

## EXPERIMENTAL SECTION

**Cell Lines.** Sarcoma 180 cells [S180, American Type Culture Collection (ATCC)] from mouse ascites were expanded in Dulbecco's Modified Eagle's Medium (DMEM) supplemented with 1% (v/v) penicillin–streptomycin mixtures and 10% (v/v) fetal bovine serum (FBS, Hyclone) in culture incubators at 5% CO<sub>2</sub> and 37 °C.

**Chemical Reagents.** The chemical compounds, including paclitaxel (PTX, MedChemExpress) and hematoporphyrin IX dihydrochloride (HP, MedChemExpress), were employed for the preparation of carrier-free nanodrugs. Indocyanine Green (ICG, SigmaAldrich) as a fluorescent dye was used to monitor the structural integrity of nerve fibers. Hydrogel made of sodium hyaluronate (HA, MedChemExpress) was harnessed to simulate tumor stromal environments in ex vivo administration experiments. The bilayer of the HA hydrogel consisted of an upper layer of 2% (w/w) hydrogel and a lower one [7% (w/w)] at a volume ratio of 1:4.

**Characterization and Preparation of PTX-HP Nanoparticles.** Briefly, 5 mg of HP and 20 mg of PTX compounds had dissolved together in DMSO solvent (0.5 mL), followed by the addition of sodium hydroxide (0.9 mg). Subsequently, the mixtures were slowly dropped into 9.5 mL of 0.9% (w/w) NaCl solution comprising 0.01% (w/w) polyvinylpyrrolidone (PVP, Sigma Aldrich) while stirring vigorously to facilitate NPs' formation. Afterward, the raw NP solution was centrifuged at 2000g for 10 min so as to exclude large-sized NPs and then dialyzed in a condition of a cutoff molecular weight of 14 kDa against ultrapure water overnight. Finally, the resulting nanodrugs were stored at 4 °C after lyophilization. PTX release from nanodrugs was inspected using dialysis bags against PBS plus 10% FBS under cutoff molecular weight of 100 kDa. The PTX contents outside dialysis bags and in purified nanodrugs were detected by high-performance liquid chromatography (HPLC, Agilent). Moreover, in accordance to the manufacturer's experimental protocol, we utilized a highly sensitive Flow NanoAnalyzer (NanoFCM) to quantify the absolute amount of purified NPs. Besides, in a 96-well plate, S180 cells were cultured at a density of 5000 cells each well for 24 h. Then, the cells were incubated with different concentrations of NPs or PTX agents for 24 h, and cellular viability was further measured by cell counting kits (CCK-8, Abcam) under absorbance at 460 nm.

**Animal Studies.** The Laboratory Animal Center of Southern Medical University provided female BALB/c mice, which were purchased at similar weights and ages (7 to 8 weeks). BALB/c mice were maintained in a specific pathogen-free environment with appropriate humidity and temperature as well as light-dark cycles. All study procedures were approved by the Institutional Animal Care and Use Committee (IACUC) of the Southern Medical University and complied with the relevant regulations of IACUC. All animal behavioral assays were conducted in a period of the light cycle.

**Mouse Models of Neuropathic Cancer Pain.** As reported elsewhere,<sup>33–35</sup> the female BALB/c mice that had similar weight were selected, anesthetized with isoflurane, and subjected to surgical operation for the exposure of sciatic nerves in right leg. Subsequently, S180 tumor cells ( $5 \times 10^5$ , 20 μL) together with matrigel (BD) at a volume ratio of 1:1 were injected to the muscles in close contact to the sciatic nerves around mouse trochanter in hind legs. Finally, the wounds were closed layer by layer. In contrast, a sham procedure was carried out in other healthy mice where pure matrigel containing no sarcoma cells was injected into muscular tissues following the exposure of sciatic nerves.

The growth changes of orthotopic sarcomas were observed and quantified by ultrasonic imaging (Veo2100, Visualsonics) with multifrequency signal transducers (MS400) under a B-mode. When

the sarcoma sizes raised up to around 300 mm<sup>3</sup>, the mice that had similar weight were randomly distributed into specific groups ( $n = 5$  per group) and received an insertion by puncture needles (PTC, 23 G × 100 mm) under US imaging guidance. Then, the intratumoral infusion of nanodrugs, PBS, or free PTX plus HP was performed through the use of injection pumps at a flow rate of 5 μL s<sup>-1</sup>. Consequently, the maximum distances on lateral-medial (LM), superior-inferior (SI), and anterior-posterior (AP) planes of sarcoma masses were recorded at predetermined time points after administration using US imaging. Tumor sizes in the cancer pain model were quantified based on the previously reported equation:<sup>35</sup> tumor volume =  $(0.5 \times LM) \times (0.5 \times SI) \times (0.5 \times AP) \times (1.33 \times \pi)$ .

**Correlation Analysis between NP Doses and Tumor Volume Reduction ( $V_{\text{reduction}}$ ).** When the volume of orthotopic sarcomas reached around 300 mm<sup>3</sup> measured by US imaging, the cancer pain models received intratumoral infusion of various amounts of nanodrugs (including  $0.4025 \times 10^{10}$ ,  $0.805 \times 10^{10}$ ,  $1.61 \times 10^{10}$ ,  $3.22 \times 10^{10}$ , and  $4.83 \times 10^{10}$  NPs) by injection pumps. After the single administration, the maximum reduction in tumor volume ( $V$ ) was recorded by echography, and linear regression analysis was also conducted between NP amounts ( $N_{\text{NP}}$ ) and tumor volume reduction ( $V_{\text{reduction}}$ ) to obtain the linear regression equation ( $Y = 3.405e-009 \times X + 36.43$ ;  $\kappa = 3.405e-009$ ).

To inspect the reliability of the linear regression equation on tumor eradication, the mice bearing cancer pain (with about 300 mm<sup>3</sup> of tumors *in situ* as well as similar body weight) were i.t. administrated with a single dose of PBS, free PTX + HP, or nanodrugs under the navigation of US imaging at 8 days postinoculation. The injected doses of NPs were, respectively, 0.8-fold, 1.0-fold, and 1.2-fold of the basic NP numbers ( $N_{\text{NP}}$ ) calculated from the linear regression equation. [ $Y = 3.405e-009 \times X + 36.43$ ;  $\kappa = 3.405e-009$ ; tumor volume ( $Y$  value) is 300 and  $X$  value, namely, basic NP numbers (doses), can be obtained as a benchmark dose through using the function. Finally, the  $X$  value is  $7.741 \times 10^{10}$  NPs.] The administrated dose of free PTX plus HP was equivalent to 1.2-fold of the basic  $N_{\text{NP}}$ , which was 91 μg of PTX together with 54 μg of HP in DMSO.

**Behavioral Studies in Cancer Pain Models.** As described earlier, another batch of cancer pain models that had similar weight was established and randomly divided into three groups ( $n = 8$  per group) including: (1) PBS group, (2) free PTX + HP group, and (3) NP group, followed by i.t. infusion with PBS, free PTX + HP, or basic dose of nanodrugs (1.0×) by US imaging (when tumor size approximated to 300 mm<sup>3</sup>). Then, the treated mice were subjected to diverse behavioral assays. All mice required a habituation to experimental environments for at least 45 min prior to behavioral tests. The researchers who conducted the behavioral tests knew nothing about details of those studies. Double-blind behavioral experiments were also carried out in subsequent assays.

Spontaneous pain detection was conducted in tumor-bearing mice prior to or after i.t. injection of PBS, free PTX + HP, or basic dose of NPs ( $1.0 \times$  the basic dose =  $7.741 \times 10^{10}$  NPs), as previously described.<sup>33,34</sup> At designed time points postinoculation, the cumulative duration of paw-lifting behavior of mice was recorded in an observation period of 10 min, but grooming behavior was excluded. After that, mechanical hypersensitivity (allodynia) of ipsilateral and contralateral paws was also evaluated in Von Frey tests, where the mice stayed in a clear cage with wire-mesh bottoms for acclimation before testing. Briefly, at 0, 8, 10, 12, and 14 days after tumor inoculation, the underneath of hind paws on wire-mesh floors was stimulated with various Von Frey filaments (Semmes-Weinstein monofilaments, Stoelting Co.) that could produce a series of mechanical forces ranging from 0.04 to 2.00 g.<sup>36–38</sup> Fifty percent paw withdrawal thresholds of the treated mice were calculated on the basis of the Up&Down method according to manufacturer's instructions.<sup>39</sup> An interval of 3 min among all stimulations was required for restoration of mouse conditions.

In addition, the cold hyperalgesia of the treated mice was investigated by applying cold acetone to plantar surfaces of hind paws. As reported elsewhere,<sup>36</sup> mice demanded a habituation for at least 45 min until they were fully familiar with testing environments.

Next, approximately 25  $\mu\text{L}$  of cold acetone in a syringe barrel was dropped onto the plantar surfaces of mouse paws. Paw withdrawal frequency during a 1 min observation period was monitored after acetone stimulation. Syringe barrels without a needle should not be in contact with mouse paws to prevent the impact of other mechanical stimuli.

On Day -1, 11, and 13 following tumor inoculation, by using rotarod assays, the cancer pain models treated with PBS, PTX plus HP, or a basic dose of NPs were also observed to test their general motor functions. In brief, each mouse was observed on a rotating rod (IITC Life Sciences), and the duration spent on the rotary rod was obtained.<sup>40</sup> In rotarod assays, the rotary speeds of rods raised from 0 to 15 rpm during a period of 5 min.<sup>41</sup> Footprint tests were also harnessed to assess the basic function of the sciatic nerve in affected legs. In this test, the plantar surfaces of affected paws were soaked in dark ink, and then the mice walked on blank papers along a straight line. Ultimately, walking tracks left on those papers were carefully surveyed to calculate sciatic nerve function indexes (SFIs) as previously described,<sup>40,42</sup> which were capable of reflecting basic motor functions of sciatic nerves after various treatments.<sup>43–45</sup>

#### Biosafety Testes for the Precision Tumor Killing Treatment.

When all behavioral tests were accomplished on the 16th day after inoculation, fluorescent dye ICG (at a dose of 2 mg  $\text{kg}^{-1}$ ) dissolved in 100  $\mu\text{L}$  of normal saline was injected into muscular tissues adjacent to the affected sciatic nerves around the mouse trochanter. Eight hours after ICG administration, five out of eight mice in the behavioral tests were sacrificed and dissected to harvest various mouse organs, sciatic nerves, and tumor residues following different treatments. Afterward, parts of the resected sciatic nerves were homogenized and measured by fluorescent spectrometers (PerkinElmer) to quantify ICG fluorescence intensities in nerves. Other resected organs and tumors as histological sections received a staining treatment with hematoxylin and eosin (H&E) to compare differences among all groups.

In other biosafety studies, healthy BALB/c mice with similar body weight were intramuscularly (i.m.) injected with NPs (1.0  $\times$  the basic dose =  $7.741 \times 10^{10}$  NPs) or equivalent dose of PTX plus HP (76  $\mu\text{g}$  of PTX together with 45  $\mu\text{g}$  of HP in DMSO). Subsequently, mouse body weight was recorded every two days, and hematological tests involved in AST, ALT, urea nitrogen concentration, MCHC, HGB, lymphocyte, and RBC levels were conducted at predetermined time points postadministration ( $n = 5$  each group).

**Determination of PTX Biodistribution.** Another batch of cancer pain model that had similar weight was exploited as described above and then divided randomly into two groups ( $n = 21$  per group) receiving an i.t. infusion of nanodrugs [basic dose (1.0 $\times$ )] or free PTX plus HP (dissolved in DMSO). After the interventional administration under sonography piloting, *in vivo* PTX biodistribution was detected by LC-MS/MS analysis (Thermo Scientific, TSQ) as previously described.<sup>46</sup> In brief, three mice from each group were chosen and euthanized to collect requisite biosamples (i.e., blood, sciatic nerves, mouse organs, and tumors) at designed time points. Through employing a homogenizer device, biosamples were first homogenized in Dulbecco's Phosphate Buffered Saline and extracted with aliquots of tertiary butyl methyl ether (TBME, 5 mL) at 4 °C. After vortexing for over 25 min, the mixture was further centrifuged for 30 min at 4 °C (2000g) to separate the organic layer from aqueous phases. Next, the organic solution was placed carefully into a clear tube and evaporated under nitrogen streaming. Finally, the residues in tubes were redissolved in methanol (150  $\mu\text{L}$ ), followed by measurements through LC-MS/MS analysis. Notably, docetaxel was added to the tissue homogenate as an internal standard. To confirm extraction efficiencies, homogenate of biosamples in healthy control mice required an addition of exogenous PTX.

**Statistical Analysis.** Statistical analysis was carried out utilizing GraphPad Prism 8. For comparison of two group, an unpaired two-tailed *t* test was employed for assessing statistical differences. A two-way analysis of variance (ANOVA) was also used for difference comparison among multiple groups. We harnessed Mantel-Cox tests to evaluate the statistical significance in survival studies. All data

presented in a form of means  $\pm$  standard deviation (SD), and \**P* < 0.05 was considered to be statistically significant.

#### ASSOCIATED CONTENT

##### Data Availability Statement

All data are available in this paper or Supporting Information. Correspondence and further requests for materials should be addressed to Li Ma, Xiaoyuan Chen, or Pengfei Zhang.

##### SI Supporting Information

The Supporting Information is available free of charge at <https://pubs.acs.org/doi/10.1021/acsnano.3c06511>.

Supplemental Figure S1: Characterization of PTX-HP nanodrugs *in vitro*; Supplemental Figure S2: Representative H&E-stained sections of S180 sarcoma in orthotopic cancer pain models i.t. infused with PBS, PTX plus HP, or NPs; Supplemental Figure S3: Measurements of biosafety in healthy mice after administration (PDF)

#### AUTHOR INFORMATION

##### Corresponding Authors

Pengfei Zhang – Institute of Molecular Immunology, School of Laboratory Medicine and Biotechnology, Southern Medical University, Guangzhou 510000, China;  [orcid.org/0000-0003-1186-5950](https://orcid.org/0000-0003-1186-5950); Email: [zpf0418@smu.edu.cn](mailto:zpf0418@smu.edu.cn)

Xiaoyuan Chen – Departments of Diagnostic Radiology, Surgery, Chemical and Biomolecular Engineering, and Biomedical Engineering, Clinical Imaging Research Centre, Nanomedicine Translational Research Program, Yong Loo Lin School of Medicine and Faculty of Engineering, National University of Singapore, Singapore 699010, Singapore;  [orcid.org/0000-0002-9622-0870](https://orcid.org/0000-0002-9622-0870); Email: [chen.shawn@nus.edu.sg](mailto:chen.shawn@nus.edu.sg)

Li Ma – Institute of Molecular Immunology, School of Laboratory Medicine and Biotechnology, Southern Medical University, Guangzhou 510000, China; Email: [mali\\_61648322@smu.edu.cn](mailto:mali_61648322@smu.edu.cn)

##### Authors

Sheng Yao – Guangdong Provincial Key Laboratory of Medical Image Processing, Guangdong Province Engineering Laboratory for Medical Imaging and Diagnostic Technology, School of Biomedical Engineering, Southern Medical University, Guangzhou 510000, China

Yu Tang – Institute of Molecular Immunology, School of Laboratory Medicine and Biotechnology, Southern Medical University, Guangzhou 510000, China

Shanhe Wan – Guangdong Provincial Key Laboratory of New Drug Screening, School of Pharmaceutical Science, Southern Medical University, Guangzhou 510000, China

Complete contact information is available at:

<https://pubs.acs.org/10.1021/acsnano.3c06511>

##### Author Contributions

P.Z., X.C., and L.M. designed the researches; P.Z. and X.C. wrote this paper. P.Z., S.Y., Y.T., and S.W. performed the experiments and analyzed data. L.M. and X.C. supervised the research.

##### Funding

This work was supported by Natural Science Foundation of Anhui Province (2008085QH383, P.Z.), Provincial key laboratory of immune regulation and immunotherapy

(2022B1212010009, L.M.), Guangdong Basic and Applied Basic Research Foundation (2023A1515012356, P.Z.), and Guangzhou Basic and Applied Basic Research Foundation (202201011237, P.Z.).

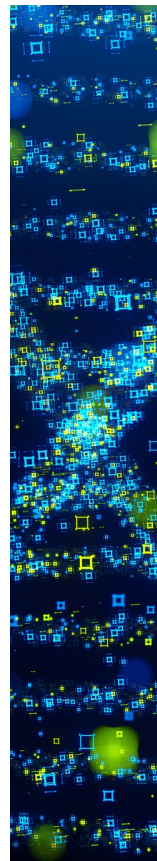
## Notes

The authors declare no competing financial interest.

## REFERENCES

- (1) Lara-Solares, A.; Ahumada Olea, M.; Basantes Pinos, A. L. A.; Bistre Cohen, S.; Bonilla Sierra, P.; Duarte Juarez, E. R.; Simon Escudero, O. A.; Santacruz Escudero, J. G.; Flores Cantisani, J. A. Latin-American guidelines for cancer pain management. *Pain Manag*. **2017**, *7* (4), 287–298.
- (2) van den Beuken-van Everdingen, M. H. J.; de Rijke, J. M.; Kessels, A. G.; Schouten, H. C.; van Kleef, M.; Patijn, J. High prevalence of pain in patients with cancer in a large population-based study in The Netherlands. *Pain*. **2007**, *132* (3), 312–320.
- (3) Villars, P.; Dodd, M.; West, C.; Koetters, T.; Paul, S. M.; Schumacher, K.; Tripathy, D.; Koo, P.; Miaskowski, C. Differences in the prevalence and severity of side effects based on type of analgesic prescription in patients with chronic cancer pain. *J. Pain Symptom Manage*. **2007**, *33* (1), 67–77.
- (4) Neufeld, N. J.; Elnahal, S. M.; Alvarez, R. H. Cancer pain: a review of epidemiology, clinical quality and value impact. *Future Oncol*. **2017**, *13* (9), 833–841.
- (5) Fink, R. M.; Gallagher, E. Cancer Pain Assessment and Measurement. *Semin Oncol Nurs*. **2019**, *35* (3), 229–234.
- (6) Rojo, R. D.; Ren, J. L.; Lipe, D. N.; Badr, H.; Shete, S.; Hanna, E. Y.; Reyes-Gibby, C. C. Neuropathic pain prevalence and risk factors in head and neck cancer survivors. *Head Neck*. **2022**, *44* (12), 2820–2833.
- (7) Brown, D.; Krebs, H.; Brower, J.; O'Hara, R.; Wang, E.; Vaheesan, K.; Du, L.; Matsuoka, L.; D'Souza, D.; Sze, D. Y.; Golzarian, J.; Gandhi, R.; Kennedy, A. Incidence and risk factors for sustained hepatic function toxicity 6 months after radioembolization: analysis of the radiation-emitting SIR-spheres in non-resectable liver tumor (RESIN). *registry. J. Gastrointest Oncol*. **2021**, *12* (2), 639–657.
- (8) Wong, T. Y.; Zhang, K. S.; Gandhi, R. T.; Collins, Z. S.; O'Hara, R.; Wang, E. A.; Vaheesan, K.; Matsuoka, L.; Sze, D. Y.; Kennedy, A. S.; Brown, D. B. Long-term outcomes following 90Y Radioembolization of neuroendocrine liver metastases: evaluation of the radiation-emitting SIR-spheres in non-resectable liver tumor (RESiN) registry. *BMC Cancer*. **2022**, *22* (1), 224.
- (9) Deng, G. Integrative Medicine Therapies for Pain Management in Cancer Patients. *Cancer J.* **2019**, *25* (5), 343–348.
- (10) Spahn, V.; Del Vecchio, G.; Labuz, D.; Rodriguez-Gaztelumendi, A.; Massaly, N.; Temp, J.; Durmaz, V.; Sabri, P.; Reidelbach, M.; Machelska, H.; Weber, M.; Stein, C. A nontoxic pain killer designed by modeling of pathological receptor conformations. *Science*. **2017**, *355* (6328), 966–969.
- (11) Preux, C.; Bertin, M.; Tarot, A.; Authier, N.; Pinol, N.; Brugnon, D.; Pereira, B.; Guastella, V. Prevalence of Opioid Use Disorder among Patients with Cancer-Related Pain: A Systematic Review. *J. Clin. Med.* **2022**, *11* (6), 1594.
- (12) Hao, X.; Zhou, Y.; Ling, Y.; Miyoshi, H.; Sumitani, M.; Chan, K. Y.; Park, H. J.; Feng, Z.; Rao, Y. Effects of high-dose opioid analgesia on survival, pain relief, quality of life and adverse drug reactions in cancer and neuropathic pain patients: a retrospective cohort study in real-world clinical practice. *Ann. Transl. Med.* **2022**, *10* (18), 998.
- (13) Bhansali, D.; Teng, S. L.; Lee, C. S.; Schmidt, B. L.; Bunnett, N. W.; Leong, K. W. Nanotechnology for Pain Management: Current and Future Therapeutic Interventions. *Nano Today*. **2021**, *39*, No. 101223.
- (14) Peptu, C.; Rotaru, R.; Ignat, L.; Humelnicu, A. C.; Harabagiu, V.; Peptu, C. A.; Leon, M. M.; Mitu, F.; Cojocaru, E.; Boca, A.; Tamba, B. I. Nanotechnology approaches for pain therapy through transdermal drug delivery. *Curr. Pharm. Des.* **2015**, *21* (42), 6125–39.
- (15) Chakravarthy, K. V.; Boehm, F. J.; Christo, P. J. Nanotechnology: A Promising Paradigm for the Control of Pain. *Pain Med*. **2018**, *19* (2), 232–243.
- (16) Chen, J.; Jin, T.; Zhang, H. Nanotechnology in Chronic Pain Relief. *Front. Bioeng. Biotechnol.* **2020**, *8*, 682.
- (17) Zhang, P.; Xiao, Y.; Sun, X.; Lin, X.; Koo, S.; Yaremenko, A. V.; Qin, D.; Kong, N.; Farokhzad, O. C.; Tao, W. Cancer nanomedicine toward clinical translation: Obstacles, opportunities, and future prospects. *Med*. **2023**, *4* (3), 147–167.
- (18) Xie, L. S.; Li, J.; Wang, G. H.; Sang, W.; Xu, M. Z.; Li, W. X.; Yan, J.; Li, B.; Zhang, Z.; Zhao, Q.; Yuan, Z.; Fan, Q. L.; Dai, Y. L. Phototheranostic Metal-Phenolic Networks with Antixosomal PD-L1 Enhanced Ferroptosis for Synergistic Immunotherapy. *J. Am. Chem. Soc.* **2022**, *144* (2), 787–797.
- (19) Yan, J.; Wang, G. H.; Xie, L. S.; Tian, H.; Li, J.; Li, B.; Sang, W.; Li, W. X.; Zhang, Z.; Dai, Y. L. Engineering Radiosensitizer-Based Metal-Phenolic Networks Potentiate STING Pathway Activation for Advanced Radiotherapy. *Adv. Mater.* **2022**, *34* (10), No. e2105783.
- (20) Zhang, J. Q.; Zhu, S. S.; Tan, Q. L.; Cheng, D.; Dai, Q. Q.; Yang, Z. L.; Zhang, L.; Li, F. F.; Zuo, Y. M.; Dai, W.; Chen, L. H.; Gu, E. W.; Xu, G. H.; Wei, Z. L.; Cao, Y. X.; Liu, X. S. Combination therapy with ropivacaine-loaded liposomes and nutrient deprivation for simultaneous cancer therapy and cancer pain relief. *Theranostics*. **2020**, *10* (11), 4885–4899.
- (21) Mercadante, S.; Bruera, E. Methadone as a First-Line Opioid in Cancer Pain Management: A Systematic Review. *J. Pain Symptom Manag*. **2018**, *55* (3), 998–1003.
- (22) van den Beuken-van Everdingen, M.H.J.; de Rijke, J.M.; Kessels, A.G.; Schouten, H.C.; van Kleef, M.; Patijn, J. Prevalence of pain in patients with cancer: a systematic review of the past 40 years. *Annals of Oncology*. **2007**, *18* (9), 1437–1449.
- (23) Haugen, D. F.; Hjermstad, M. J.; Hagen, N.; Caraceni, A.; Kaasa, S. Epcrc, Assessment and classification of cancer breakthrough pain: A systematic literature review. *Pain*. **2010**, *149* (3), 476–482.
- (24) Arthur, J. A.; Reddy, A.; Smith, U.; Hui, D.; Park, M.; Liu, D.; Vaughan-Adams, N.; Haider, A.; Williams, J.; Bruera, E. Practices and perceptions regarding intravenous opioid infusion and cancer pain management. *Cancer*. **2019**, *125* (21), 3882–3889.
- (25) Anderson, K. O.; Mendoza, T. R.; Valero, V.; Richman, S. P.; Russell, C.; Hurley, J.; DeLeon, C.; Washington, P.; Palos, G.; Payne, R.; Cleeland, C. S. Minority cancer patients and their providers: pain management attitudes and practice. *Cancer*. **2000**, *88* (8), 1929–38.
- (26) Yang, Y.; Yan, J.; Huang, Y.; Xu, H.; Zhang, Y.; Hu, R.; Jiang, J.; Chen, Z.; Jiang, H. The cancer pain related factors affected by celecoxib together with cetuximab in head and neck squamous cell carcinoma. *Biomed. Pharmacother*. **2015**, *70*, 181–9.
- (27) Vendrell, I.; Macedo, D.; Alho, I.; Dionisio, M. R.; Costa, L. Treatment of Cancer Pain by Targeting Cytokines. *Mediators Inflamm*. **2015**, *2015*, 1–11.
- (28) Zhang, Q. Q.; Shi, D. W.; Guo, M. Q.; Zhao, H.; Zhao, Y. B.; Yang, X. L. Radiofrequency-Activated Pyroptosis of Bi-Valent Gold Nanocluster for Cancer Immunotherapy. *Acs Nano*. **2023**, *17* (1), S15–S29.
- (29) Tian, Z.; Hu, Q. T.; Sun, Z. Y.; Wang, N.; He, H. L.; Tang, Z.; Chen, W. Y. A Booster for Radiofrequency Ablation: Advanced Adjuvant Therapy via Nanovaccine Synergized with Anti-programmed Death Ligand 1 Immunotherapy for Systemically Constraining Hepatocellular Carcinoma. *Acs Nano*. **2023**, *17* (19), 19441–19458.
- (30) Shimoyama, M.; Tatsuoka, H.; Ohtori, S.; Tanaka, K.; Shimoyama, N. Change of dorsal horn neurochemistry in a mouse model of neuropathic cancer pain. *Pain*. **2005**, *114* (1–2), 221–30.
- (31) Liu, Y. P.; Shen, B.; Liu, F.; Zhang, B.; Chu, T. W.; Bai, J.; Bao, S. L. Synthesis, radiolabeling, biodistribution and fluorescent imaging of histidine-coupled hematoporphyrin. *Nucl. Med. Biol.* **2012**, *39* (4), 579–585.
- (32) Sehgal, I.; Sibrian-Vazquez, M. Photoinduced cytotoxicity and biodistribution of prostate cancer cell-targeted porphyrins. *J. Med. Chem.* **2008**, *51* (19), 6014–6020.

- (33) Shimoyama, M.; Tanaka, K.; Hasue, F.; Shimoyama, N. A mouse model of neuropathic cancer pain. *Pain* **2002**, *99* (1–2), 167–74.
- (34) Zhang, J.; Zhu, S.; Tan, Q.; Cheng, D.; Dai, Q.; Yang, Z.; Zhang, L.; Li, F.; Zuo, Y.; Dai, W.; Chen, L.; Gu, E.; Xu, G.; Wei, Z.; Cao, Y.; Liu, X. Combination therapy with ropivacaine-loaded liposomes and nutrient deprivation for simultaneous cancer therapy and cancer pain relief. *Theranostics* **2020**, *10* (11), 4885–4899.
- (35) Albadawi, H.; Zhang, Z. F.; Altun, I.; Hu, J. J.; Jamal, L.; Ibsen, K. N.; Tanner, E. E. L.; Mitragotri, S.; Oklu, R. Percutaneous liquid ablation agent for tumor treatment and drug delivery. *Science Translational Medicine* **2021**, *13* (580), No. eabe3889.
- (36) Moreno, A. M.; Aleman, F.; Catroli, G. F.; Hunt, M.; Hu, M.; Dailamy, A.; Pla, A.; Woller, S. A.; Palmer, N.; Parekh, U.; McDonald, D.; Roberts, A. J.; Goodwill, V.; Dryden, I.; Hevner, R. F.; Delay, L.; Goncalves Dos Santos, G.; Yaksh, T. L.; Mali, P. Long-lasting analgesia via targeted in situ repression of Na(V)1.7 in mice. *Sci Transl Med* **2021**, *13* (584), No. eaay9056.
- (37) Au, M. T.; Shi, J. Y.; Fan, Y. D.; Ni, J. G.; Wen, C. Y.; Yang, M. Nerve Growth Factor-Targeted Molecular Theranostics Based on Molybdenum Disulfide Nanosheet-Coated Gold Nanorods (MoS-AuNR) for Osteoarthritis Pain. *Acs Nano* **2021**, *15* (7), 11711–11723.
- (38) Xie, X.; Pascual, C.; Lieu, C.; Oh, S.; Wang, J.; Zou, B. D.; Xie, J. L.; Li, Z. H.; Xie, J.; Yeomans, D. C.; Wu, M. X.; Xie, X. S. Analgesic Microneedle Patch for Neuropathic Pain Therapy. *Acs Nano* **2017**, *11* (1), 395–406.
- (39) Chen, G.; Kim, Y. H.; Li, H.; Luo, H.; Liu, D. L.; Zhang, Z. J.; Lay, M.; Chang, W.; Zhang, Y. Q.; Ji, R. R. PD-L1 inhibits acute and chronic pain by suppressing nociceptive neuron activity via PD-1. *Nat Neurosci* **2017**, *20* (7), 917–926.
- (40) Wei, J.; Su, W.; Zhao, Y.; Wei, Z.; Hua, Y.; Xue, P.; Zhu, X.; Chen, Y.; Chen, G. Maresin 1 promotes nerve regeneration and alleviates neuropathic pain after nerve injury. *J. Neuroinflammation* **2022**, *19* (1), 32.
- (41) Chen, G.; Park, C. K.; Xie, R. G.; Ji, R. R. Intrathecal bone marrow stromal cells inhibit neuropathic pain via TGF-beta secretion. *J. Clin. Invest.* **2015**, *125* (8), 3226–40.
- (42) Su, W. F.; Wu, F.; Jin, Z. H.; Gu, Y.; Chen, Y. T.; Fei, Y.; Chen, H.; Wang, Y. X.; Xing, L. Y.; Zhao, Y. Y.; Yuan, Y.; Tang, X.; Chen, G. Overexpression of P2 × 4 receptor in Schwann cells promotes motor and sensory functional recovery and remyelination via BDNF secretion after nerve injury. *Glia* **2019**, *67* (1), 78–90.
- (43) Cazuza, R. A.; Batallé, G.; Bai, X.; Leite-Panissi, C. R. A.; Pol, O. Effects of treatment with a carbon monoxide donor and an activator of heme oxygenase 1 on the nociceptive, apoptotic and/or oxidative alterations induced by persistent inflammatory pain in the central nervous system of mice. *Brain Res. Bull.* **2022**, *188*, 169–178.
- (44) Deer, T. R.; Eldabe, S.; Falowski, S. M.; Huntoon, M. A.; Staats, P. S.; Cassar, I. R.; Crosby, N. D.; Boggs, J. W. Peripherally Induced Reconditioning of the Central Nervous System: A Proposed Mechanistic Theory for Sustained Relief of Chronic Pain with Percutaneous Peripheral Nerve Stimulation. *J. Pain. Res.* **2021**, *14*, 721–736.
- (45) Di Carlo, M.; Bianchi, B.; Cipolletta, E.; Farah, S.; Filippucci, E.; Salaffi, F. Imaging of the peripheral nervous system in nociceptive pain: An ultrasound study in patients with fibromyalgia. *J. Neuroimaging* **2023**, *33* (4), 558–565.
- (46) Layek, B.; Sadhukha, T.; Panyam, J.; Prabha, S. Nano-Engineered Mesenchymal Stem Cells Increase Therapeutic Efficacy of Anticancer Drug Through True Active Tumor Targeting. *Mol. Cancer Ther.* **2018**, *17* (6), 1196–1206.



CAS BIOFINDER DISCOVERY PLATFORM™

## STOP DIGGING THROUGH DATA — START MAKING DISCOVERIES

CAS BioFinder helps you find the right biological insights in seconds

Start your search

**CAS**   
A division of the  
American Chemical Society